FM-Aided Heuristic Drift Reduction for Pedestrian Dead Reckoning Systems

Haidong Wang, Li Cong, and Honglei Qin

Abstract—**Accurate indoor pedestrian positioning has attracted extensive research attention along with the rising popularity of indoor location-based service. Among the indoor positioning methods, pedestrian dead reckoning stands out for requiring neither expensive infrastructure nor laborious site survey. However, with time going on, the pedestrian dead reckoning method suffers from error accumulation problem, whereas the major cause of positioning error is usually heading deviation. To tackle the error-drifting problem, an FM-aided heuristic drift reduction method for pedestrian dead reckoning systems is designed and evaluate in this paper. First a random forest classifier is devised to achieve real-time recognition of straight-line and turning motion mode with data from frequency-modulated radio signal and inertial sensor signal. Based on the classification result, constraint is applied to headings in straight periods and accurate headings are extracted from accelerometer and magnetometer measurements to reduce heading deviation in straight periods. Field experiments have been conducted at three sites in two office buildings to evaluate the performance of the proposed system. Experiment results indicate error drifting can be effectively constrained by the proposed method.**

Index Terms—**indoor positioning; pedestrian dead reckoning; microelectromechanical sensor; frequency modulation; pattern recognition.**

I. Introduction

G REAT application potential lies in indoor location-based service (LBS) for its integration of precise positioning and related service. With the aid of indoor LBS, people are able to quickly determine their position and find the optimal route for their target location in large venues like supermarkets and museums. In outdoor regions, Global Navigation Satellite System (GNSS) has been the de facto standard positioning approach after decades of development. However, myriad walls, doors, furniture, together with frequent human activity, cause GNSS signal to suffer from severe attenuation and multipath in indoor environment, resulting in its failure of normal functioning. Consequently, indoor positioning systems have to rely on other methods to provide user location. Indoor positioning systems can be categorized by technique into four major types as concluded by [1]: lateration/angulation systems [2]–[5], proximity systems [6], [7], radio fingerprinting systems [8]–[11] and dead reckoning systems [12]–[18]. In comparison to the other three types of positioning techniques, dead reckoning systems are featured for being highly infrastructure-free.

Dead reckoning systems can be classified into two categories: inertial navigation system (INS) and pedestrian dead reckoning (PDR). The INS approach provides user position by integrating acceleration in the global coordinate system (GCS) whereas the PDR approach adds up displacement vector of each step to locate users. Owing to the double integration in INS, quickly accumulated error could result in tremendous position drift for systems using sensors manufactured with microelectromechanical systems (MEMS) technology. Therefore, to restrict error drifting, practical INS-based pedestrian positioning systems have to fix sensor units to the feet of users and apply specialized constraints like zero velocity update and zero angular rate update [1], [13], [19]. On the other hand, such requirement about sensor attachment is not compulsory for PDR systems, where sensors can be placed in various places like hand, pocket and bag. Usually a PDR system can be divided into three major parts: step detection, step length estimation and heading estimation. Step detection can be achieved by detecting the cyclic peaks in acceleration measurements produced by human movement with methods, like peak detection, based on the difference between moving and motionless standing [12], [20], [21], or methods making use of the periodical pattern like zero crossing detection and autocorrelation [1], [22]. For step length estimation, some formulas [23]–[25] have been put forward with reported high accuracy, taking account of acceleration, walking frequency, and other possible factors [26], [27]. Heading can be derived from integration of gyroscope, which is the same as the INS scheme. In addition, magnetometers, which are often included in smartphones, can be utilized to estimate attitude of the device together with accelerometer, as an approach independent from gyroscope. These two independent methods of computing user heading can be integrated together to get better estimations [14], [16].

Dead reckoning positioning systems feature high independence from the environment, requiring neither complicated device deployment nor laborious site survey. However, error drifting still remains a serious problem for dead reckoning methods in spite of years of research in this area, especially when low-cost MEMS sensors in smartphones are chosen as measuring tool. Of the three major parts of the PDR approach, error drifting in heading could result in the largest trajectory error. On the other hand, it has been proposed that many corridors inside buildings share the style of straight line [28], a useful feature for heuristic drift reduction methods [29]–[35]. Therefore, in this paper, a pedestrian positioning system is devised to tackle the error-drifting problem with the aid of the straight-line feature in indoor environments. To utilize the

straight-line feature, accurate classification of straight-line and curve segments in the tracks is required. Sensor measurements like angular velocity are usually employed for the classification task. Meanwhile we can also take advantage of other signals like frequency-modulated (FM) signal to improve the classification result while maintaining sufficient independence from the external environment. Thanks to the fact that wavelength of FM signal, around 3 meters, are comparable to the size of common indoor equipment, FM signal is confronted with much less attenuation than other high-frequency signals like GNSS and WiFi signals while propagating in indoor environment. FM signal characteristics at one position, also known as signal fingerprint in fingerprinting systems [36]–[38] vary across indoor space. Thus different signal variation trend might be detected while walking on different routes. This feature is utilized to integrate FM signal strength measurements and MEMS sensor measurements to recognize straight and turning moments.

In this paper, an FM-aided heuristic drift reduction method for PDR systems is proposed and evaluated. The method performs classification of straight and turning moments and improves heading estimation in straight segments to produce accurate positioning results. Accurate classification of straight/turning mode is completed by a random forest classifier with FM RSSI data and MEMS sensor data collected by a smartphone. Then a reliability selection scheme is employed to filter aberrant magnetic measurements and select the reliable ones, from which final headings of straight-line segments are extracted. Experiments have been performed to evaluate the performance of the proposed drift reduction method. It's illustrated by the experiments that error drifting can be effectively constrained by the proposed method.

The rest of the paper is organized as follows: in Section II the details are described of step detection, step length estimation, motion mode classification, and heading estimation. Then performance of the system is analyzed and evaluated by practical field experiments in Section III. Finally conclusions and future works are summarized in Section IV.

II. System Design

A. System Architecture

Overall architecture of the system proposed in this paper is illustrated as Fig. 1. Acceleration signal is used to detect step events and count the number of steps, together with the estimation of step length. Headings are divided into two parts: headings of straight-line periods and headings of turning periods. Classification of turning and straight-line periods is implemented by a random forest classifier with data from FM receiver, accelerometer, gyroscope and magnetometer. Headings of straight-line periods are estimated with only magnetic data, whereas headings of turning periods are estimated with measurements from gyroscope. Finally, trajectory is generated with estimation results of step number, step lengths, and headings.

B. Coordinate Transformation & Attitude Computation

Direct output of three-axis MEMS sensors are expressed in the local coordinate system (LCS), whereas positions and other navigation information are usually given in GCS. As has been stated in previous literatures [39], [40], transformation from GCS to LCS can be achieved by a rotation matrix R:

$$
\begin{aligned}
R &= \begin{bmatrix} c\gamma & 0 & -s\gamma \\ 0 & 1 & 0 \\ s\gamma & 0 & c\gamma \end{bmatrix} \begin{bmatrix} 1 & 0 & 0 \\ 0 & c\theta & s\theta \\ 0 & -s\theta & c\theta \end{bmatrix} \begin{bmatrix} c\psi & -s\psi & 0 \\ s\psi & c\psi & 0 \\ 0 & 0 & 1 \end{bmatrix} \\
&= \begin{bmatrix} c\gamma c\psi + s\gamma s\theta s\psi & -c\gamma s\psi + s\gamma s\theta c\psi & -s\gamma c\theta \\ c\theta s\psi & c\theta c\psi & s\theta \\ s\gamma c\psi - c\gamma s\theta s\psi & -s\gamma s\psi - c\gamma s\theta c\psi & c\gamma c\theta \end{bmatrix}
\end{aligned}
\tag{1}
$$

, where c denotes cos function, s denotes sin function, ψ denotes the heading (also referred to as yaw angle), θ denotes the pitch angle, and γ is the roll angle. The x axis of GCS points to the east, the y axis points to the north and the z axis points upward. If a vector in LCS needs to be converted to GCS, the corresponding rotation matrix would be the transpose of R.

In a specific place, we may deem the gravity vector and the magnetic field vector as constant in a short period. Thus, when the device stays static or moves with a constant speed, accelerometer and magnetometer directly measure the projections of the gravity vector and magnetic field vector. This provides us with the opportunity to attain attitude angles of the device with these two sensors as followed:

$$
\theta = \operatorname{atan2} \frac{a_y}{\sqrt{a_x^2 + a_z^2}}
\tag{2a}
$$

$$
\gamma = \operatorname{atan2} \frac{-a_x}{a_z}
\tag{2b}
$$

$$
\psi = \operatorname{atan2} \frac{m_x c\gamma + m_z s\gamma}{m_y c\theta + m_x s\theta s\gamma - m_z s\theta c\gamma} + \delta
\tag{2c}
$$

, where $[a_x, a_y, a_z]$ is the acceleration measurement in LCS, $[m_x, m_y, m_z]$ is the magnetic field strength measurement in LCS, δ is the regional constant magnetic declination , c denotes cos function, and s denotes sin function.

In this way we can get complete attitude angles of the device with an accelerometer and a magnetometer, although theoretical accuracy is only guaranteed when the device is static or moving with a constant speed, and magnetic interference should be nearly zero. In fact, experiments in this paper are conducted with a mobile phone carried in front of the chest of the test taker. And the experiment taker walks at a normal constant speed without high dynamics. Therefore estimation in this method is reliable to some extent [16]. Moreover, this calculation method is free from cumulative error, which is an advantage not possessed by the angular integration method.

C. Step Detection & Counting

Step detection is completed with z-axis acceleration data in GCS by a mixed method combining zero crossing, threshold detection, and duration constraint. Acceleration in z-axis of GCS is selected due to its insensitiveness to device posture while exhibiting cyclic oscillation pattern in the walking process. Output data from accelerometer are first smoothed with a low-pass filter to remove irregular noise. The low-pass filter we used is a 300-order equiripple finite impulse response
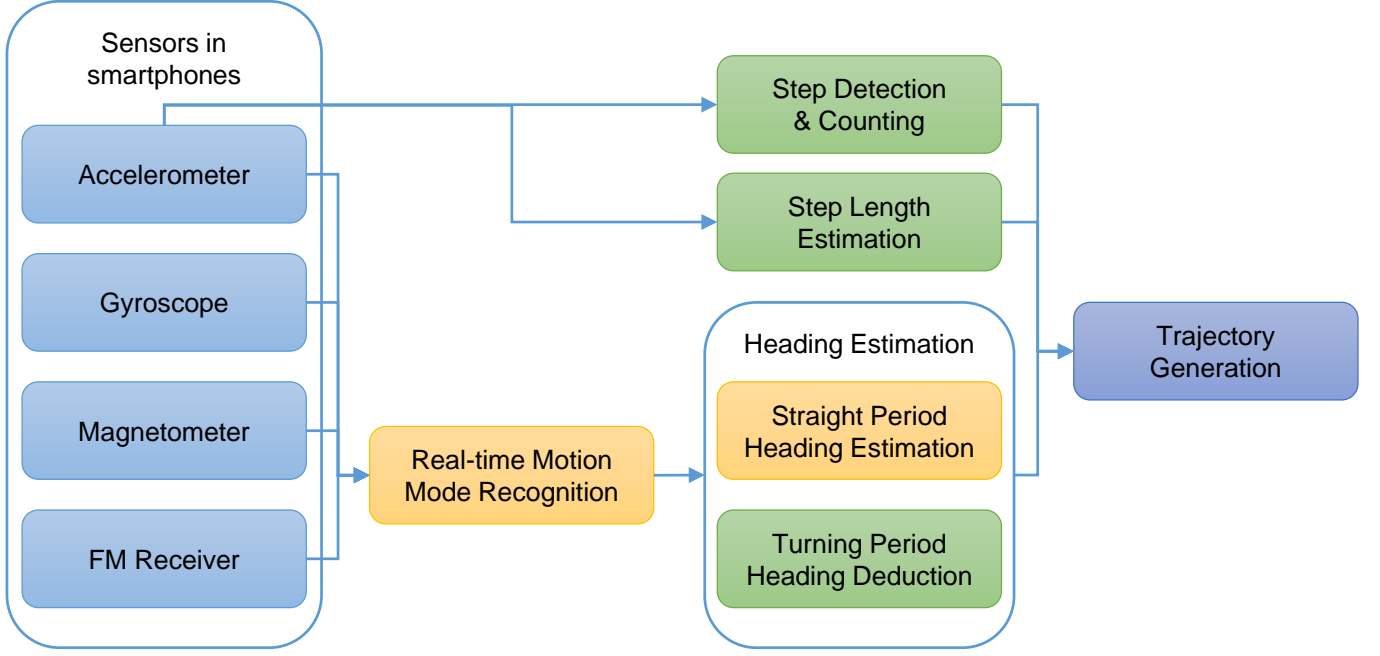
Fig. 1. Overall system architecture

filter, whose passband frequency is 3 Hz, stopband frequency is 5 Hz, passband weight and stopband weight are both 1, and density factor is 20. Then pitch and roll angles are calculated according to Equation (2a), (2b) and (2c). With pitch and roll angles, we can rotate LCS two times as described in the B part of Section II, after which positive direction of z axes in LCS and GCS become consistent. After the rotations z-axis value of acceleration is composed of gravity and vertical acceleration of the device. Estimation of the gravity vector is completed by detecting and calculating the mean value in a static period. Then the gravity component is removed and vertical acceleration of the device is extracted.

Our step detection method is similar to the method adopted by Qian [27]. The cyclic pattern of human movement produces cyclic peaks in acceleration. Thus acceleration peaks should be detected so as to count steps. Acceleration peaks begin and end with zero-crossing events, which can be expressed as below:

$$a_{p-1}^{GCS} \cdot a_p^{GCS} \leq 0 \qquad (3a)$$
$$a_q^{GCS} \cdot a_{q+1}^{GCS} \leq 0 \qquad (3b)$$

, where p is the beginning moment of the peak, q is the ending moment of the peak, a_{p-1}^{GCS}, a_p^{GCS}, a_q^{GCS}, and a_{q+1}^{GCS} are vertical acceleration values in GCS without gravity component at moment $p-1$, p, $q-1$ and q. The maximum absolute acceleration within the peak also need to be greater than a threshold:

$$\max\{|a^{GCS}|\} > a_{thres}^{GCS} \qquad (4)$$

, where a_{thres}^{GCS} is the threshold for absolute vertical acceleration in GCS without gravity component. The value of a_{thres}^{GCS} in our algorithm is $0.8\mathrm{m/s^2}$ based on observation of acceleration data and testing of the detection method. Using Equation (3

and (4) we can estimate acceleration peaks roughly. However, some of the detected peaks might last too short as a result of sensor noise. Whereas some others might last too long, and the absolute acceleration values are much smaller than the threshold a_{thres}^{GCS}. For these aberrant results, limits on step duration are essential to remove them so that the detection results are reliable, as illustrated below:

$$T_{min} \leq T \leq T_{max} \qquad (5)$$

, where T is the duration one step lasts, T_{min} is the shortest duration one step may last and T_{max} is the longest duration one step may last. Once a peak with duration shorter than T_{min}, which is 0.16 second in our algorithm, is detected, it will be regarded as false alarm and will not be taken as valid result. If a peak is detected with duration longer than threshold T_{max}, which is 1 second in our algorithm, moments after duration T_{max} would be regarded as static standing moments. Fig. 2 also provides an illustration of how this step detection method works.

With the step detection method described above, we can get the exact beginning and ending moments of each step. An example of peak and step detection result is shown in Fig. 3, where each peak/step is denoted by a non-zero value and values of neighboring peaks/steps are different in order to distinguish them. To test the accuracy of the step detection method, walking experiment was conducted on a standard 400-meter athletic track. 20 laps of sensor data were collected in 133.5 minutes and the total number of steps is 13,356. Detection result of the proposed method is 13,322 steps and the accuracy is 99.75%.
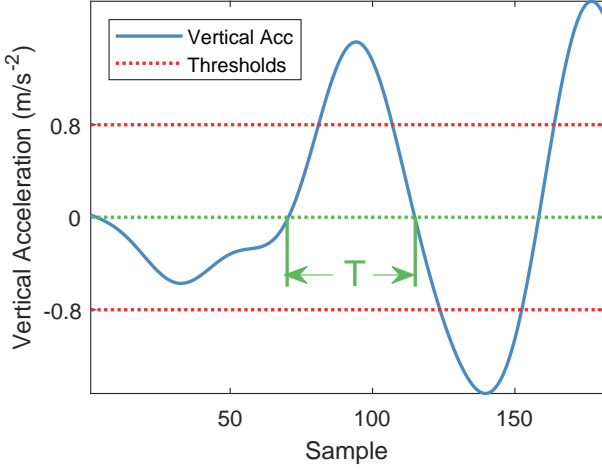
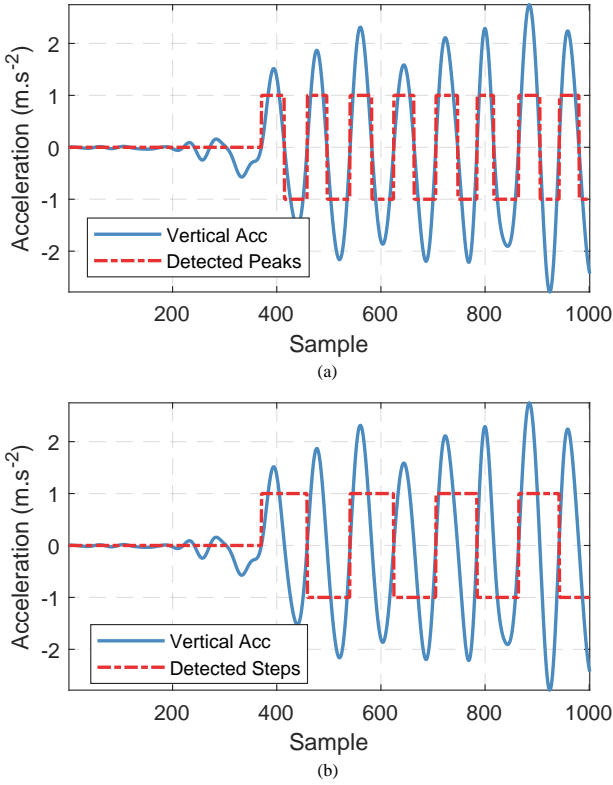Fig. 2. Illustration of our peak detection method. T is the duration of the peak.

(a)

(b)

Fig. 3. An example of peak and step detection results. (a) Detection result of acceleration peaks. (b) Detection result of steps.

D. Step Length Estimation

In the PDR scheme step length is utilized together with heading to attain the position change after one step. The length of each step is related to multiple factors: variation in acceleration, walking frequency, pedestrian height etc. In this paper, the Weinberg approach [23] is adopted to estimate step length. Based on simplification of human walking motion, the Weinberg approach estimates the length of a stride, the process of taking one step by one leg and a following step by another, as the following equation:

$$d = k \cdot \sqrt[4]{a_{max} - a_{min}} \qquad (6)$$

, where d is the length of one stride (consecutive two steps), k is an empirical constant, a_{max} and a_{min} are the maximal and minimal vertical acceleration value. The value of k, which is $0.90 \, \mathrm{m}^{3/4} \cdot \mathrm{s}^{1/2}$ in our algorithm, is an average value obtained from the 20-lap athletic track data. As stated in [23], step length error of this method can be restricted to no more than $\pm 8\%$.

E. Heading Estimation

Heading estimation is the most critic part of the PDR algorithm because a tiny error in heading can lead to quite large position error. The angular-integration method, which integrates angular velocity to obtain heading, and the acc-mag heading estimation method, which uses accelerometer and magnetometer to estimate heading, both suffer from problems in spite of unique advantages. For the angular-integration method, integration result is reliable within short durations yet cumulative error could deteriorate positioning accuracy after long time. As for the acc-mag method, it is free from error accumulation but vulnerable to magnetic distortion in indoor environment.

Inside buildings many paths like corridors are straight and common human walking route tend to be straight in such paths like corridors. The straight-line feature of indoor paths can be utilized to aid the pedestrian positioning system as the HDR method [30], [34]. In this paper the straight line feature is also utilized, but the implementation is different from previous literatures. Heading estimation in this paper is composed of two steps. First a random forest classifier is designed to distinguish straight/turning moments with input of FM and sensor measurements. Then true headings of straight periods are extracted from accelerometer and magnetometer measurements based on the classification results.

1) Random Forest Classification: Indoor paths can be segmented into straight and curved parts. Straight/curved segment detection is the basis for separate processing for them. A simple way to discriminate them is to apply a threshold on the absolute value of angular velocity with respect to z-axis in GCS as the following equation:

$$|\omega^{GCS}| \geq \Omega_{thres} \qquad (7)$$

, where ω^{GCS} is the angular velocity with respect to z-axis in GCS and Ω_{thres} is the threshold for it. If there is any change in pedestrian heading, a spike of ω^{GCS} would appear and the turning would be detected, as illustrated in Fig. 4. For simplification, we refer to this method as the "threshold-detection method". Although simple and effective for high-precision inertial units, this method might fail when applied to low-cost MEMS gyroscopes due to noise interference. Curves with small curvature might also be hard to detect since change rate of heading could be very small and corresponding spikes might be submerged by noise.
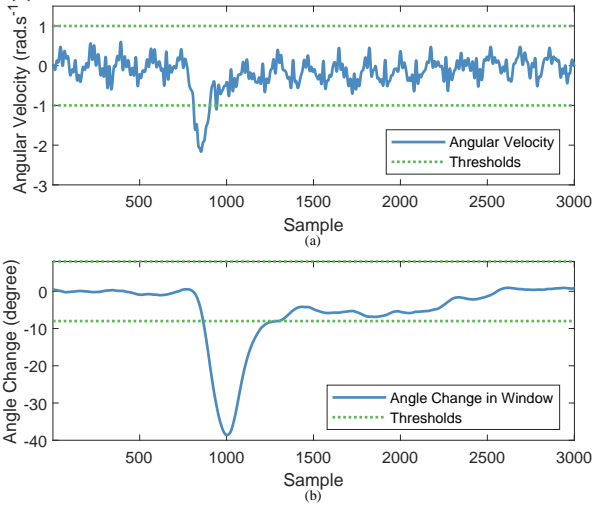
Fig. 5. A demonstration of how random forests work.

Fig. 4. Demonstration of the threshold-detection method and the window-detection method. The two subfigures are generated with the same gyroscope data input. (a) Demonstration of the threshold-detection method. (b) Demonstration of the window-detection method.

Another method is to apply a time window to the change rate of heading and compute the total change amount of heading in a time window. We refer to this method as the "window-detection method". The change amount of heading in a time window may be computed as:

$$|\psi_{end} - \psi_{begin}| \geq \psi_{thres} \tag{8}$$

, where ψ_{end} and ψ_{begin} are headings at the beginning and ending moment in the time window, ψ_{thres} is the corresponding threshold. Another way is to use the maximum heading difference in the time window:

$$\max\{|\psi_p - \psi_q|\} \geq \psi_{thres} \tag{9}$$

, where ψ_p and ψ_q are headings at arbitrary moment p and q in the time window. Once the change amount exceeds the threshold ψ_{thres}, a turning event is detected. However, delay would be introduced by this method, especially for smooth curves where long time windows are needed to make correct judgment.

Apart from MEMS sensors, there are some other components in smartphones with measuring function like the WiFi/Bluetooth/FM chip. Among the signals measurable for smartphones, FM signal can be employed to assist our detection while maintaining high independence of the system for its pervasiveness. The integration of FM and sensor data is completed by a random forest classifier. For simplification, we refer to this straight/turning detection method as the "RF-detection method".

Random forest is a learning method that achieves classification/prediction by constructing multiple decision trees and synthesizing outputs of the individual trees [41]. Fig.5 provides a demonstration of how it works. Decision tree is a tree-like structure where each non-leaf node represents one test with respect to one feature, each branch represents one test result and each leaf node represents one class label (for
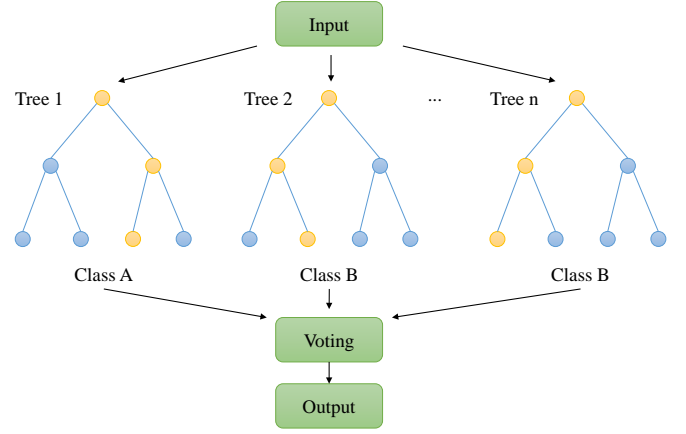
classification) or prediction (for regression). Decision trees are vulnerable to overfitting in spite of simplicity, whereas this defect can be remedied by random forest. For each decision tree in random forest, samples and features used for its training is randomly selected from the general sample and feature set. And then the majority vote of all the trees is taken as the output class label of the random forest. Thanks to the random selection of samples and features, decision trees in random forests are de-correlated and result of the forest is resistant to overfitting.

With determined data source, algorithm, and task goal, we can move to detailed procedures. Direct measurements available from smartphones are the received signal strength (RSSI) of FM radio, device acceleration, angular velocity, and magnetic field strength. Sampling rate of accelerometer, gyroscope and magnetometer are all set to 50 Hz. For the FM receiver chip, it costs about 0.1 second to tune to a new FM frequency and read RSSI, resulting in the actual sampling rate for each FM channel to decrease with the increase in channel number. Therefore, three FM channels , whose frequencies are 96.9 Hz, 102.5 Hz and 107.3 Hz, are selected for the experiments in consideration of signal strength, stability, and actual sampling rate.

To clearly describe the motion state of one specific moment, we need to extract features from input data. First we apply a sliding time window to data stream. The length of the time window is 340 samples and the data input rate is 150 Hz. The window overlap is set to 339 for sufficient training data. Then an array of 43 features are calculated:

1) Standard deviation of RSSI in the time window for each FM channel;
2) RSSI Difference of beginning and ending moment of the time window for each FM channel;
3) Maximum difference of RSSI in the time window for each FM channel;
4) Mean frequency of the spectrum of RSSI in the time window for each channel;
5) Standard deviation of auto correlation array of RSSI in the time window for each channel;
6) Difference of beginning and ending value of the auto

correlation array of RSSI in the time window for each channel;

7) Difference of maximum and minimum value of the auto correlation array of RSSI in the time window for each channel;

8) Three-axis acceleration measurement;

9) Three-axis angular velocity measurement;

10) Standard deviation of three-axis acceleration in the time window;

11) Standard deviation of three-axis angular velocity in the time window;

12) Attitude angles calculated by the angular-integration method in the time window;

13) Attitude angles calculated by the acc-mag method in the time window;

14) Standard deviation of headings calculated by the angular-integration method (1 dimension);

15) Difference of headings calculated by the angular-integration method at beginning and ending moments in the time window (1 dimension);

16) Standard deviation of heading calculated by the acc-mag method (1 dimension);

17) Difference of headings calculated by the acc-mag method at beginning and ending moment in the time window (1 dimension);

In the feature list above, except item 14 to 17, each item contains 3 dimensions of features. The incorporation of FM signal introduces new information for the random forest classifier to make decisions. Fig. 6 provides a demonstration of the differences of FM signal features in straight and turning segments. From Fig. 6 we can see that the value range and change rates of FM features at turning segments are different from those at straight moments. Therefore, we decide to use the combination of FM features and sensor features to enhance classification performance.

There are two types of labels in the output of the classifier: straight-line walking moments, when the carrier is walking in a straight line, and turning moments, when the carrier is making a turn. True labels of experiment data are generated by a modified version of the window-detection method. First the time window in the window-detection method is set long enough to tackle smooth turns in these trajectories. Then beginning moments of each turn is moved forward by 0.8 average step duration so that detection results of beginning moments are more accurate. Similarly, ending moments are moved backward by 1.5 average step duration.

2) Heading Determination: Reliable classification of straight and turning moments paves the way for separate processing of heading. The main idea of heading estimation in this paper is to restrain heading deviation in straight periods based on the assumption that headings of different moments within the same straight period stay the same. For the straight periods, heading of each step is calculated with moments when the headings are not far from the average heading of the moment. For turning periods, headings are calculated by the angular-integration method, with the beginning moments of the turning periods as the initial moment of integration.

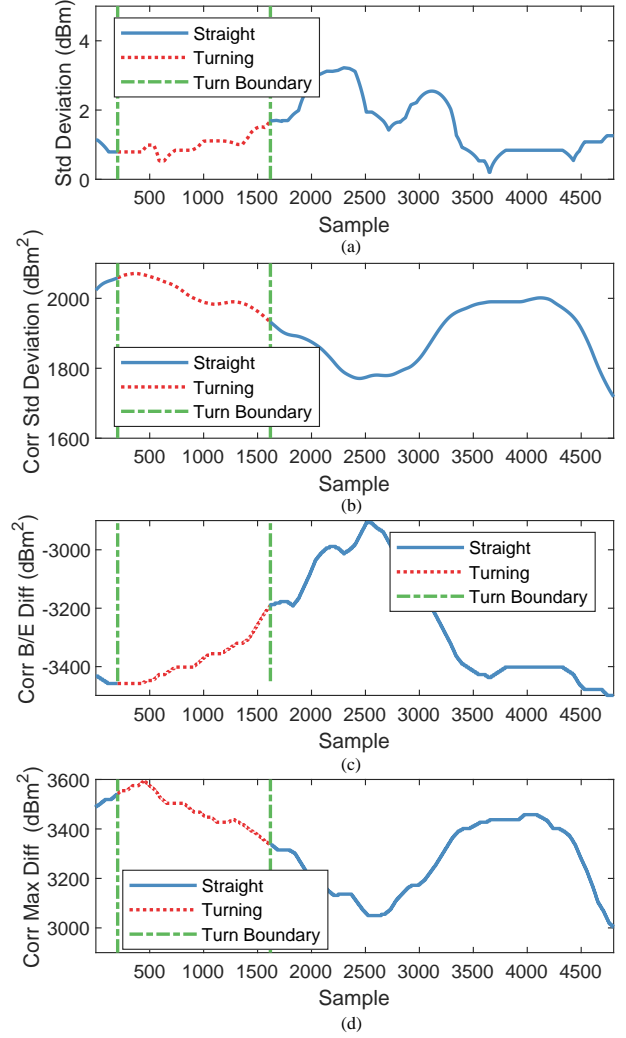To get the heading of one step in the straight period, first

Fig. 6. A demonstration of FM feature variations in straight-line and turning segments. The blue solid parts are straight segments and the red dotted part is a turning segment. (a) Standard deviation of FM RSSI in time window for channel 102.5 Hz. (b) Standard deviation of auto correlation array of RSSI in time window for channel 107.3 Hz. (c) Difference of beginning and ending value of the RSSI auto correlation array in time window for channel 102.5 Hz; (d) Difference of maximum and minimum value of the RSSI auto correlation array in time window for channel 107.3 Hz.

moment selection is conducted based on a set of criterions and then weighted average is applied to generate a reliable heading estimation for this step. At the selection stage two criterions are utilized: heading deviation from average heading of the straight period, and deviation of magnetic field strength vector from average vector of the period. The criterions are listed as followed:

$$\delta\psi_p = |\psi_p - \overline{\psi}(p_0, p)| < \psi_{thres} \qquad (10a)$$

$$\delta v_p = \langle \mathbf{M}_p, \overline{\mathbf{M}}(p_0, p) \rangle < v_{thres} \qquad (10b)$$

, where p_0 is the beginning moment of this straight period, moment p is one moment in the straight period, ψ_p is the device heading at moment p, $\overline{\psi}(p_0, p)$ is the average heading from moment p_0 to moment p, $\delta\psi_p$ is the deviation angle of device heading ψ_p from $\overline{\psi}(p_0, p)$ at moment p, ψ_{thres} is the

threshold for the heading deviation, $\mathbf{M}_p$ is the magnetic field strength vector at moment p, $\overline{\mathbf{M}}(p_0, p)$ is the average magnetic vector from moment p_0 to moment p, δv_p is the deviation angle of magnetic vector $\mathbf{M}_p$ from $\overline{\mathbf{M}}(p_0, p)$, and v_{thres} is the threshold for angular deviation of magnetic vector from the average vector $\overline{\mathbf{M}}(p_0, p)$. If threshold ψ_{thres} and v_{thres} are set too large, more data with magnetic disturbance would be regarded as normal data and it would be more difficult to obtain accurate headings. However, if the two thresholds are set too small, many data without disturbance may be filtered out and final headings may also deviate from true headings. After testing on straight-line data, we took $4°$ as the value of ψ_{thres} and $6°$ as the value of v_{thres} for best positioning accuracy. Each of the two criterions would filter out a set of qualified moments. To integrate the two sets, we tested both the intersection and union of them as the result of selection, and found that in most cases the union of the two sets would produce more accurate trajectories. Consequently union of the two sets is taken as the filtering result.

With moment selection result, we can work out a compound deviation estimation from ground truth for each moment:

$$\delta_p = w \cdot \delta\psi_p + (1 - w) \cdot \delta v_p \tag{11}$$

, where δ_p is the compound deviation of moment p and w is the weight of $\delta\psi_p$. To fit with different deviation range of ψ_p and v_p, the value of w changes dynamically as illustrated below:

$$w = \frac{m_v}{m_v + m_\psi} \tag{12}$$

, where

$$m_\psi = \max\{\delta\psi_p\} - \min\{\delta\psi_p\} \tag{13a}$$

$$m_v = \max\{\delta v_p\} - \min\{\delta v_p\} \tag{13b}$$

Then final heading of moment p is calculated by weight averaging of headings:

$$\psi_p^{final} = \sum_{q=p_0}^{p} \frac{\psi_q}{\delta_q} \Bigg/ \sum_{q=p_0}^{p} \frac{1}{\delta_q} \tag{14}$$

, where ψ_p^{final} is the final heading of moment p. The constraints on magnetic heading deviation and magnetic vector deviation, together with heading estimation result, is shown in Fig. 7, where we can know that magnetic interference can cause severe deviation in heading, and headings calculated from gyroscope data may also drift away from ground truth after some time. Whereas our heading estimation method is able to filter out interfered magnetic measurements and yield accurate and stable heading estimations.

Theoretically deviation in heading or magnetic strength vector at one specific moment should be evaluated with true value in the period, whereas what we can obtain are measurements with noise and interference. Thus a practical solution is to take the average value of the whole period as estimation of true value. However, future data are not available in the midst of one period, leading us to use the average from the beginning moment of the period to current moment as alternative. Such substitution would of course introduce error as cost of real-time processing. With time going on, such error
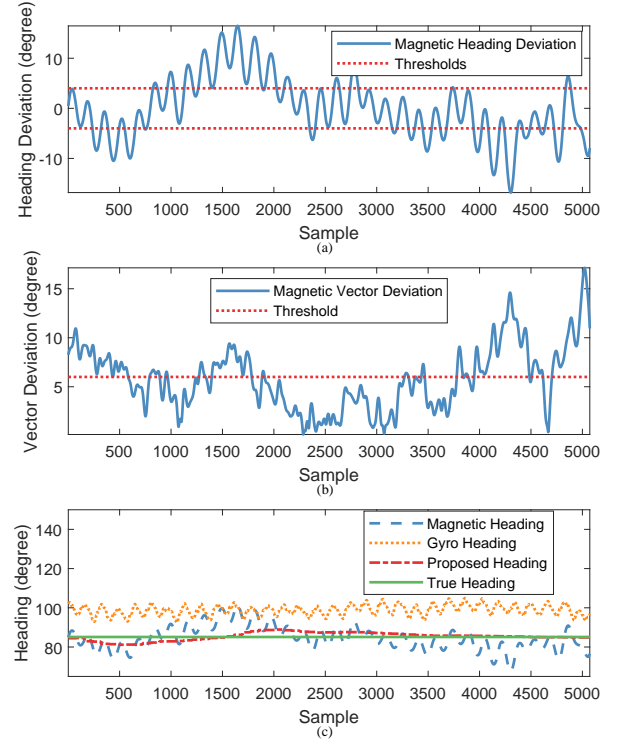

Fig. 7. An example of heading constraint and heading estimation in a straight-line segment. (a) Magnetic heading deviation and corresponding thresholds. (b) Magnetic vector deviation and corresponding threshold. (c) Heading estimation result of different methods.

gradually decreases since more and more information about the period is collected and mean value of collected data would be increasingly close to average of the whole period. This can also be proved by Fig. 7, in which the heading deviation of our proposed method grows smaller and smaller with time going on. What's more, calculation for heading of one moment might be burdensome for smartphones. A simple way to ease the burden is to only carry out such calculation at the ending moment of each step.

Headings of turning periods may keep changing, leaving much less space for constraints. Therefore, headings of turning moments are calculated by the angular-integration method. Integration in one turning period starts from the beginning moment of that period. Initial attitude is the same as the attitude at the end of last straight period. In this way, attitude deduction is restarted and error drifting is reset to zero every time a new turning period starts. Moreover, all the sensor data in last straight period can be devoted to get a better estimation of initial heading.

3) Trajectory Generation: Commonly in a PDR scheme, trajectory generation is a step-by-step deduction process:

$$\begin{bmatrix} x_p \\ y_p \end{bmatrix} = \begin{bmatrix} x_{p-1} \\ y_{p-1} \end{bmatrix} + l_p \begin{bmatrix} s\psi_p \\ c\psi_p \end{bmatrix} \tag{15}$$

, where x_p and y_p are the distances from the initial location in the direction of x and y axis at step p, x_{p-1} and y_{p-1} are the distances at step $p - 1$, l_p is the length of step p, ψ_p
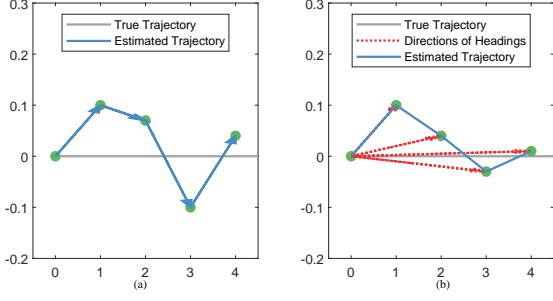
Fig. 8. Example of different trajectory generation methods with the same data input. (a) Common trajectory generation method. (b) Proposed trajectory generation method in straight-line segments.

is the heading of step p, c is the cos function and s is the sin function. However in our system, modification is made to the trajectory generation method described above so as to fully utilize the assumption that headings of moments in one straight period stay the same. In this paper, position at step p in a straight period is determined by the following equation:

$$\begin{bmatrix} x_p \\ y_p \end{bmatrix} = \begin{bmatrix} x_{p_0-1} \\ y_{p_0-1} \end{bmatrix} + \sum_{q=p_0}^{p} l_q \cdot \begin{bmatrix} s\psi_p \\ c\psi_p \end{bmatrix} \qquad (16)$$

, where step p_0 is the first step of this straight period, x_{p_0-1}, y_{p_0-1} are the coordinates of the last step of the previous turning period, c is the cos function and s is the sin function. Fig.8 provides an example of how the two trajectory generation methods work with the same input. As shown in Fig.8, the movement vector pointing to the position of the followed step start from current step, which is the case of the common method. However, in our method the movement vector pointing to position of the followed step always starts from position of the first step in current straight-line segment. Positions of steps in turning periods are still deduced with equation (15). As steps in a straight period increases, more sensor data can be gathered and heading estimation error declines gradually, which would significantly reduce trajectory error.

III. EXPERIMENTS & RESULT ANALYSIS

A. Experiment Setup

Field experiments have been designed and conducted to evaluate the performance of the drift reduction method proposed in this paper. Two aspects are involved in the experiments: evaluation of random forest classifier and assessment of trajectory error.

Experiment data are collected using a Xiaomi Redmi 4 smartphone with built-in accelerometer, gyroscope, magnetometer, and FM receiver. Sampling rate of acceleration, angular velocity, and magnetic field strength are all 50 Hz, whereas the average interval for an FM signal strength measurement to update is 0.117 microsecond. The smartphone is held by the test taker in front of the chest while walking, as shown in Fig.9.

Fig. 9. An demonstration of test taker holding the smartphone while collecting data. (a) Front view. (b) Side view.

B. Random Forest Classification Experiment

1) Classification Performance: Classification of straight and turning moments is the basis for heading dirft reduction in this paper. Due to the incorporation of FM signal, the performance of the classifier may be affected by both test site and trajectory shape. Therefore, walking data made up of different trajectory segments at five sites are collected to verify the classification performance of the proposed random forest calssifier. At each site, 5 laps of data was collected and the trajectories consist of straight-line segments, $90°$ sharp turns and smooth turns with radius up to 6 m. Lengths of turns take up 16.6% to 29.2% of the total trajectory lengths at the five sites, and overall proportion of turn length in total trajectory length 22.6%. It took 30.9 minutes in all to collect the data for classifier verification.

The k-fold cross validation method is employed in this paper to prove the peformance of the classifier. Here we use 5-fold cross validation and data in each fold consists of data at one site. Each time one fold is selected for test and the other folds are used for model training. Each random forest consists of 50 decision trees after testing and minimal number of observations per tree leaf is 30 to avoid overfitting.

Classification result of all the samples at the 5 test sites is shown as Table I, from which we can know that 91.42% of the turning moments are correctly classified and 98.14% of the straight moments are correctly recognized. The overall classification accuracy is 96.47% for all the samples.

To identify the contribution of FM signal in the classification test above, experiment has also been conducted with FM related features removed for both train and test data. Corresponding classification results are presented in Table II. By comparing Table I and Table II we can find that classification accuracy of turning moments can get an improvement of 3.0% with the aid of FM features, whereas the improvement in accuracy of straight-line moments is 0.6%. Error cost of turning moments tends to contribute more to final trajectory error than that of straight-line moments. If part of a straight-line period were wrongly recognized as turning

TABLE I
CONFUSION MATRIX OF CLASSIFICATION RESULT, WITH FM FEATURES

	Turning (Truth)	Straight (Truth)	
Turning (Detected)	62978	3868	94.21%
Straight (Detected)	5910	204198	97.19%
	91.42%	**98.14%**	**96.47%**

TABLE II
CONFUSION MATRIX OF CLASSIFICATION RESULT, WITHOUT FM FEATURES

	Turning (Truth)	Straight (Truth)	
Turning (Detected)	61094	5093	92.31%
Straight (Detected)	7794	202973	96.30%
	88.69%	**97.55%**	**95.35%**

Fig. 10. Sample curve (the red solid segment) used for turn detection.

Fig. 11. Turn detection result of the threshold-detection method.

period, heading deduction scheme would fall back to angular integration, the result of which is reliable within a short period. However, if part of a turning period were misclassified as straight-line period, heading of each moment in this period would be recognized as the same value, resulting in severe location deviation. Thus, improvement in turning segment classification accuracy can make substantial contribution to positioning error elimination. Consequently, the classification accuracy improvement for turning mode presented in Table I and Table II provides support for the contribution of FM signal, which would be further substantiated in the location determination experiment.

2) Real-time Detection: The proposed random forest classifier is able to determine whether current moment is straight or turning accurately without data from future moments. For comparison of real-time detection, we tested the proposed RF-detection method together with the aforementioned threshold-detection method and the window-detection method. To highlight the case, we selected a curve segment for detection demonstration as illustrated in Fig. 10. The radius of the sample curve is 6 m and it begins with a 90° sharp turn and ends smoothly in the end.

All of the three detection methods are all applied to detect this curve. First a threshold is applied to the z-axis angular rate in GCS. Angular rate in the z-axis in GCS and related detection result of the threshold-detection method is shown in Fig. 11, where the positive label represents straight line walking moments and negative label denotes turning moments. The first moment of the curve is sample 810 and the last moment is sample 2110. The threshold-detection method can only detect the initial sharp turn and it fails to detect the following smoothly turning moments. Detection results of the window-detection method are illustrated in Fig. 12, where two time windows with different length are tested for comparison. First a short time window with the duration of one average step is tested. The first subfigure in Fig. 12 shows that only part of the arc segment is detected. As comparison, in the second subfigure the whole arc is successfully detected with a time window of doubled length. For arcs with smaller curvature than the sample arc, longer time window is needed for successful detection, making it difficult to produce reliable
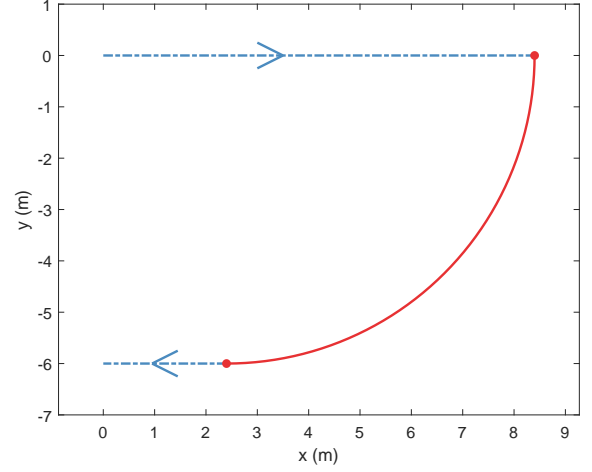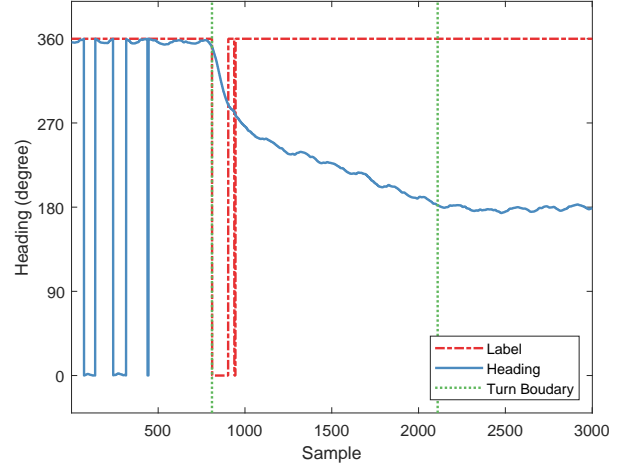
detection result within one step. Finally the proposed RF-detection method is tested, and the turn detection result is illustrated in Fig. 13, where its shown that the whole curve is successfully detected. Moreover, the detected happening moments of curve beginning and ending by these methods are listed in Table III, and the determination moments of curve beginning/ending getting detected are listed in Table IV. It is delay in the window-detection method that makes the two tables different. Based on the figures and tables, we can draw the conclusion that the proposed RF-detection method has achieved successful real-time detection of the whole arc.

C. Location Determination

Positioning performance of the proposed PDR system is evaluated by positioning experiment at three different test sites, the first two of which in one building and the third in another. At each site, 10 laps of walking data were collected and four positioning methods are compared. Total trajectory lengths at the three sites are correspondingly 1287.60 m, 662.50 m, and

TABLE III
DETECTED HAPPENING MOMENT OF CURVE BEGINNING/ENDING

Event Type	Threshold-detection	Window-detection (short window)	Window-detection (long window)	RF-detection	Ground Truth
Curve Beginning	810	866	867	814	810
Curve Ending	944	1205	2100	2097	2110

TABLE IV
DETERMINATION MOMENT OF CURVE BEGINNING/ENDING GETTING DETECTED

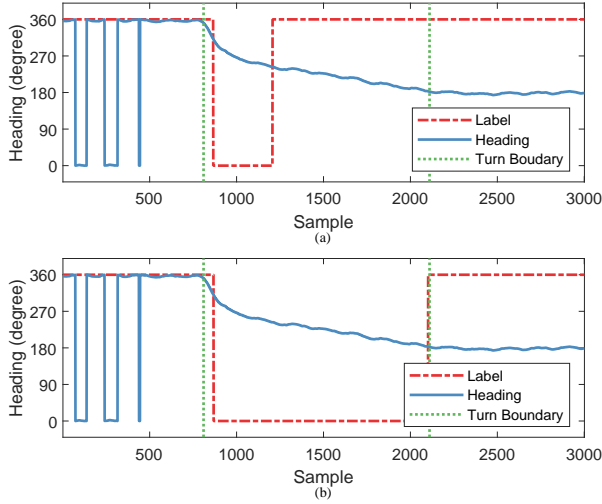| Event Type	Threshold-detection	Window-detection (short window)	Window-detection (long window)	RF-detection	Ground Truth
Curve Beginning	810	866	867	814	810
Curve Ending	944	1290	2270	2097	2110

Fig. 12. Turn detection result of the window-detection method with different time windows. (a) Duration of the time window is 1 average step; (b) Duration of the time window is 2 average steps.
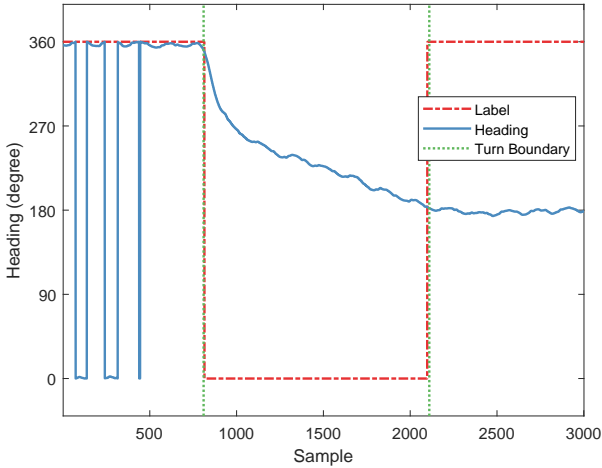

Fig. 13. Turn detection result of the RF-detection method.

4340.00 m. The differences among the first three positioning methods are the straight-line constraint method and the heading estimation method. For simplification, we refer to the first positioning method as the "gyro-heading method", the second as the "RF-sensor-only method" and the third as the "RF-FM-sensor method". A random forest classifier with all the sensor related features listed in Section II is applied in both the gyro-heading and the RF-sensor-only method. The difference between these two is the heading estimation method. For the gyro-heading method, headings are obtained by the angular-integration method in addition to an averaging operation for headings in straight-line periods. Headings in the RF-sensor-only method are computed by the proposed heading estimation method. However, the difference between the RF-sensor-only method and the RF-FM-sensor method is the motion mode classifier. The random forest classifier in the RF-FM-sensor method utilizes not only the sensor related features but also FM related ones. The fourth method, which we refer to as the "UKF method" for the usage of unscented kalman filter, is implemented according to Yuan [16] for comparison with state-of-the-art approaches.

Trajectories generated by the four methods at the first site are shown in Fig. 14. Trajectory error drifts with all of the first three methods but the extent of drifting differs. For the first trajectory, error accumulates quickly as turn number increases, resulting in the trajectory to get rotated. For the second trajectory, heading no longer drifts as turn number increases with the aid of the proposed heading estimation method. However, inaccuracy in turning detection causes the disappointing performance of heading estimation in straight-line segments. As for the third trajectory, positioning error is effectively suppressed with precise classification of turning/straight periods and the proposed heading estimation method. As comparison, trajectory error of the UKF method is larger than that of the RF-FM-sensor method.

Empirical cumulative distribution functions (CDF) of each step's positioning error for the three estimated trajectories are shown in Fig. 15. From the figure it can be clearly seen that the RF-FM-sensor method outperforms the other two. 1σ, 2σ and 3σ error of these methods are concluded as Table V. It can be concluded from Table VII that 3σ error is improved by 72.12% by the RF-FM-sensor method, and 67.31% by the RF-sensor-only method in comparison to the gyro-heading method. It is the heading drift at the first site that led to such large error for the gyro-heading method. Whereas the error difference between the RF-sensor-only method and the RF-FM-sensor method is mainly caused by classification accuracy in straight-

line segments. With the usage of FM signal, the RF-FM-sensor method is able to predict users' motion mode more precisely and constrain user heading more effectively. Comparing to the UKF method, 3σ error is improve by 37.04% by the proposed RF-FM-sensor method. Accurate heading estimation of the latter method helps a lot in constraining error effectively.

For the second site, the estimated trajectories are shown in Fig. 16. Drifting of angular velocity integration result introduced by multiple turnings leads to severe deviation of the gyro-heading trajectory, even with the aid of straight-line constraint. Although positioning error of the RF-sensor-only trajectory still drifts away with the increase of turns, it is significantly smaller than that of the gyro-heading trajectory. Maximum error of the RF-FM-sensor trajectory is close to that of the RF-sensor-only method and overall error of the former is smaller than that of the latter. As for the UKF method, inaccuracy in heading estimation led to its geat positioning error.

Empirical CDF figure of each step's positioning error for these methods are shown as Fig. 17. It is illustrated that error of the RF-FM-sensor method still exceeds errors of the other three methods. 1σ, 2σ and 3σ error of these methods are also concluded as Table VI , from which we can know the RF-sensor-only method and the RF-FM-sensor method can improve 3σ error by no less than 48.23% in comparison to the gyro-heading method and 52.08% comparing to the UKF method. The RF-FM-sensor method excels the RF-sensor-only method in overall positioning accuracy the CDF curve of the former lies to the upper left of that of the latter.

Fig. 18 illustrates the estimated trajectories at the third site. First the test taker walks rightward and then turns back to return to the initial position after reaching the right boundary, then walks upward to reach the top boundary before returning, and finally complete the left branch in the same way. Total length of the route is 434.00 m. As revealed in Fig. 18, although deviation is restricted in straight periods, drifting induced by turns still drives the trajectory away.

Positioning errors of the steps in the trajectories at the third site can be assessed by the empirical CDF curves in Fig. 19, where it is shown that the proposed RF-FM-sensor method outperforms the other three. Error performance of these methods are concluded as Table VII. It can be concluded from Table VII that 3σ error of the RF-FM-sensor method is 28.82% less than that of the gyro-heading method, and the RF-sensor-only method is 25.68% less. Drift in heading is the main reason for the positioning error of the gyro-heading method at the third site. The improvement in positioning error of the RF-FM-sensor method to the UKF method is 43.13%, which is also the result of accurate heading estimation.

We have also calculated the relative positioning error, which is the ratio of maximum positioning error to total travel distance, for the trajectories at the three sites as Table VIII. From Table VIII we can know that the relative positioning error of the RF-FM-sensor method is smaller than that of the other three methods at the first and third site. The difference of maximum error of the RF-FM-sensor and the RF-sensor-only method at the second site is no larger than 0.24 m, whereas overall error performance of the former is better. Therefore,

TABLE V
POSITIONING ERROR OF DIFFERENT POSITIONING METHODS AT THE FIRST SITE

Method	1σ Error/m	2σ Error/m	3σ Error/m
Gyro-heading	13.20	27.86	35.98
RF-sensor-only	8.68	10.75	11.76
RF-FM-sensor	6.48	8.93	10.03
UKF	8.35	12.02	15.93

TABLE VI
POSITIONING ERROR OF DIFFERENT POSITIONING METHODS AT THE SECOND SITE

Method	1σ Error/m	2σ Error/m	3σ Error/m
Gyro-heading	14.23	19.79	20.88
RF-sensor-only	8.36	9.91	10.72
RF-FM-sensor	7.59	9.85	10.81
UKF	11.59	17.41	22.56

TABLE VII
POSITIONING ERROR OF DIFFERENT POSITIONING METHODS AT THE THIRD SITE

Method	1σ Error/m	2σ Error/m	3σ Error/m
Gyro-heading	34.10	49.71	62.07
RF-sensor-only	32.91	41.08	46.13
RF-FM-sensor	29.06	38.80	44.18
UKF	55.13	72.51	77.68

TABLE VIII
RELATIVE POSITIONING ERROR OF DIFFERENT POSITIONING METHODS AT THE THREE SITES

Relative Error	First Site	Second Site	Third Site
Gyro-heading	2.84%	3.17%	1.44%
RF-sensor-only	0.93%	1.62%	1.07%
RF-FM-sensor	0.78%	1.66%	1.02%
UKF	1.26%	3.44%	1.79%

it can be proved by the experiment results above that the proposed RF-FM-sensor positioning method can provide reliable positioning results and outperform state-of-the-art indoor positioning approaches.

IV. CONCLUSION

In this paper, an FM-aided heuristic drift reduction method for PDR systems is presented and evaluated. The proposed method achieves accurate classification of straight-line and turning moments using a random forest classifier with data from FM receiver and MEMS sensors in a smartphone. Based on motion mode classification, headings of straight-line segments are extracted from magnetic measurements to constrain positioning error induced by heading deviation. Experiments prove that both the proposed classifier and the heading estimation method can improve positioning accuracy, and the combination of them yields the best performance and excels state-of-the-art indoor positioning approaches. For future work, we will focus on floor change detection and its integration with current PDR system to achieve 3D positioning.
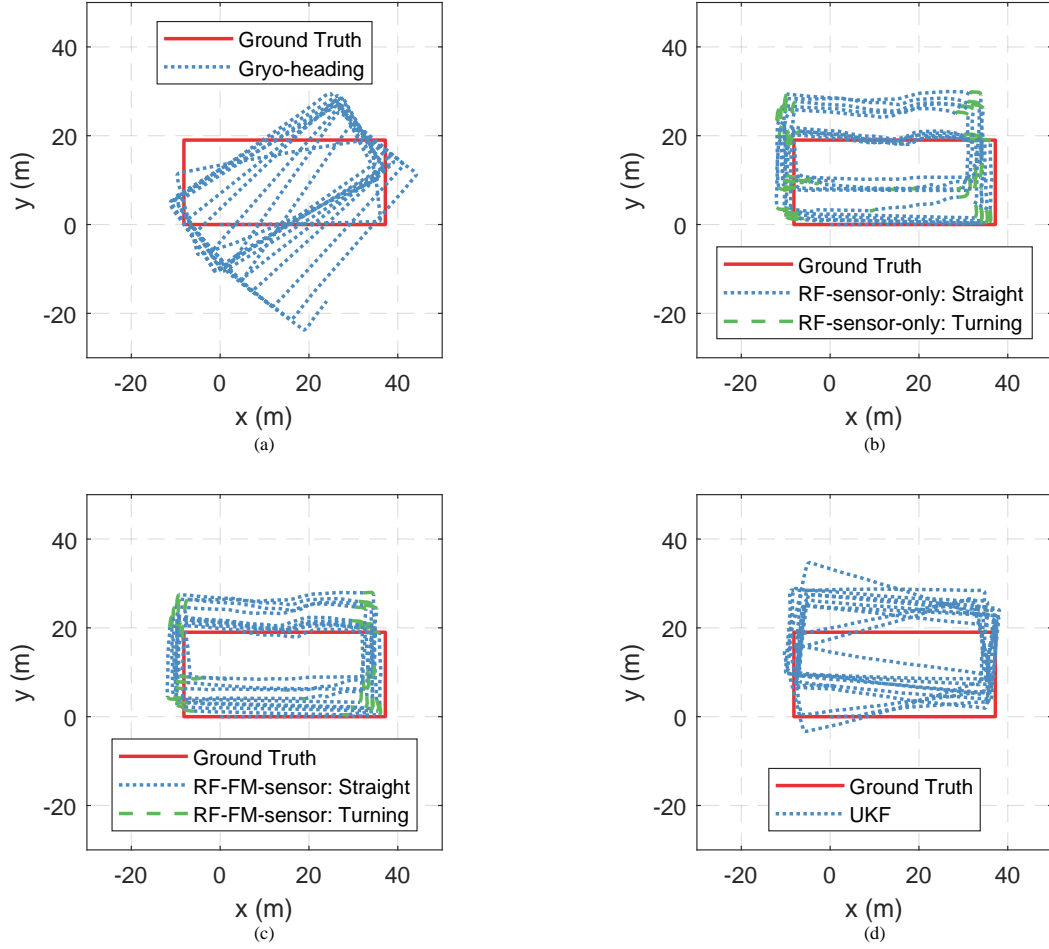
Fig. 14. Comparison of different trajectories at the first test site. (a) Trajectory by the gyro-heading method. (b) Trajectory by the RF-sensor-only method. (c) Trajectory by the RF-FM-sensor method. The blue dotted parts are detected straight-line segments and the green dash-dotted parts are detected turning segments.
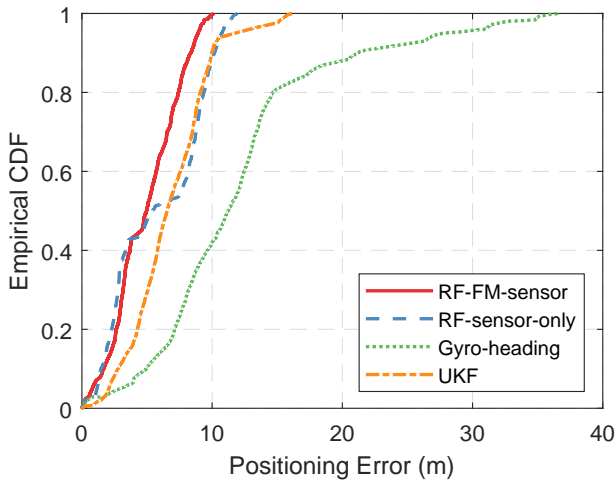
REFERENCES

[1] R. Harle, "A survey of indoor inertial positioning systems for pedestrians.," *IEEE Communications Surveys and Tutorials*, vol. 15, pp. 1281–1293, Apr. 2013.

[2] C.-D. Wann, Y.-J. Yeh, and C.-S. Hsueh, "Hybrid TDOA/AOA indoor positioning and tracking using extended kalman filters," in *2006 IEEE 63rd Vehicular Technology Conference*, vol. 3, pp. 1058–1062, May 2006.

[3] C. Yang, Y. Huang, and X. Zhu, "Hybrid TDOA/AOA method for indoor positioning systems," in *The Institution of Engineering and Technology Seminar on Location Technologies*, pp. 1–5, Dec. 2007.

[4] A. Yazici, U. Yayan, and H. Ycel, "An ultrasonic based indoor positioning system," in *2011 International Symposium on Innovations in Intelligent Systems and Applications*, pp. 585–589, June 2011.

[5] J. Tiemann, F. Schweikowski, and C. Wietfeld, "Design of an UWB indoor-positioning system for UAV navigation in GNSS-denied environments," in *2015 International Conference on Indoor Positioning and Indoor Navigation (IPIN)*, pp. 1–7, Oct. 2015.

[6] A. Bekkali, H. Sanson, and M. Matsumoto, "Rfid indoor positioning based on probabilistic RFID map and kalman filtering," in *Third IEEE International Conference on Wireless and Mobile Computing, Networking and Communications (WiMob 2007)*, pp. 21–21, Oct. 2007.

[7] S. S. Saab and Z. S. Nakad, "A standalone RFID indoor positioning system using passive tags," *IEEE Transactions on Industrial Electronics*, vol. 58, pp. 1961–1970, May 2011.

Fig. 15. Empirical error cumulative distribution functions of multiple trajectories at the first site.
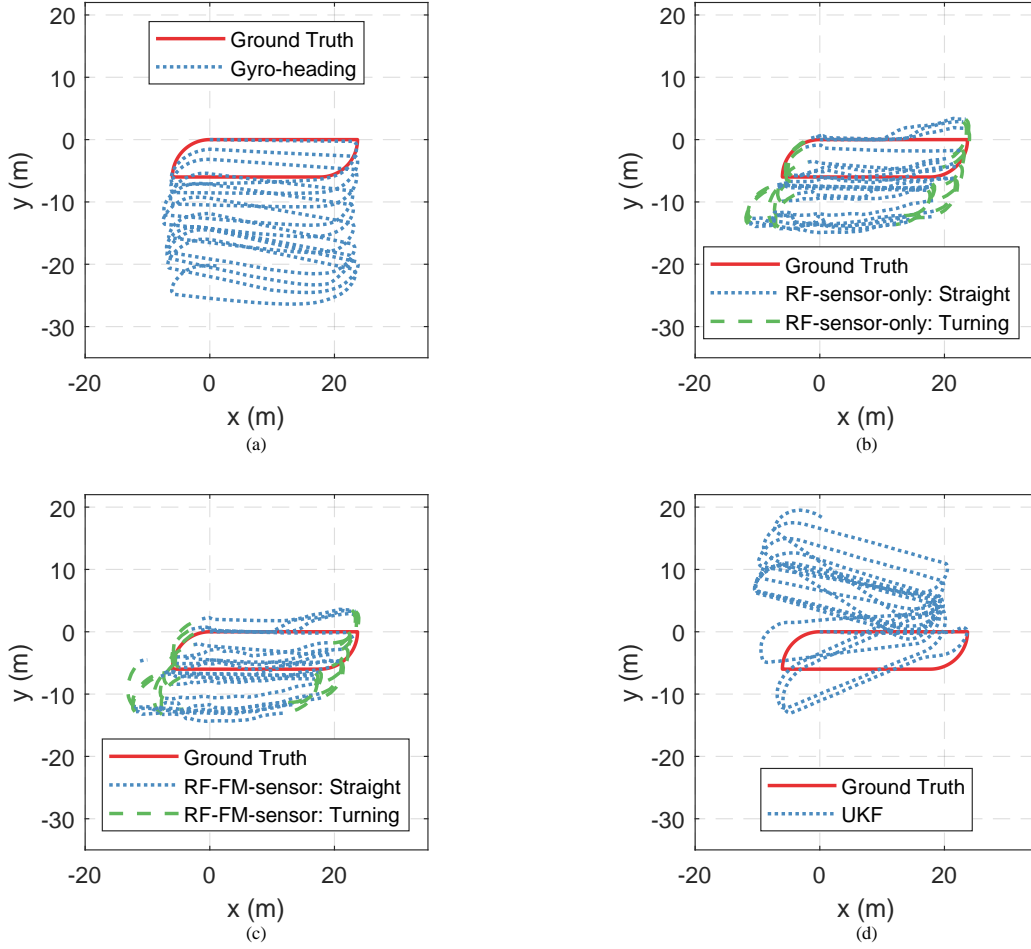
Fig. 16. Comparison of different trajectories at the second test site. (a) Trajectory by the gyro-heading method. (b) Trajectory by the RF-sensor-only method. (c) Trajectory by the RF-FM-sensor method. The blue dotted parts are detected straight-line segments and the green dash-dotted parts are detected turning segments.
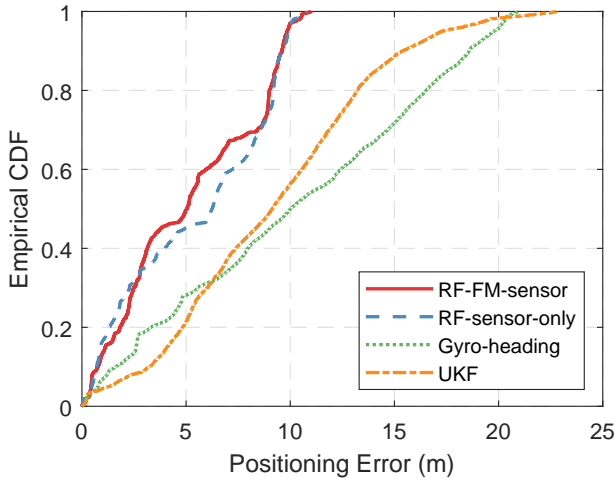

Fig. 17. Empirical error cumulative distribution functions of multiple trajectories at the second test site.

[8] S. Eisa, J. Peixoto, F. Meneses, and A. Moreira, "Removing useless APs and fingerprints from WiFi indoor positioning radio maps," in *International Conference on Indoor Positioning and Indoor Navigation*, pp. 1–7, Oct. 2013.

[9] M. N. Husen and S. Lee, "Indoor human localization with orientation using WiFi fingerprinting," in *Proceedings of the 8th International Conference on Ubiquitous Information Management and Communication*, p. 109, ACM, 2014.

[10] T. Lin, S. Fang, W. Tseng, C. Lee, and J. Hsieh, "A group-discrimination-based access point selection for wlan fingerprinting localization," *IEEE Transactions on Vehicular Technology*, vol. 63, pp. 3967–3976, Oct. 2014.

[11] S. Yiu, M. Dashti, H. Claussen, and F. Perez-Cruz, "Locating user equipments and access points using RSSI fingerprints: A Gaussian process approach," in *2016 IEEE International Conference on Communications (ICC)*, pp. 1–6, May 2016.

[12] L. Fang, P. J. Antsaklis, L. A. Montestruque, M. B. McMickell, M. Lemmon, Y. Sun, H. Fang, I. Koutroulis, M. Haenggi, M. Xie, and X. Xie, "Design of a wireless assisted pedestrian dead reckoning system - the NavMote experience," *IEEE Transactions on Instrumentation and Measurement*, vol. 54, pp. 2342–2358, Dec. 2005.

[13] P. Strömbäck, J. Rantakokko, S.-L. Wirkander, M. Alexandersson, K. Fors, I. Skog, and P. Händel, "Foot-mounted inertial navigation and cooperative sensor fusion for indoor positioning," in *ION International Technical Meeting (ITM)*, pp. 89–98, 2010.

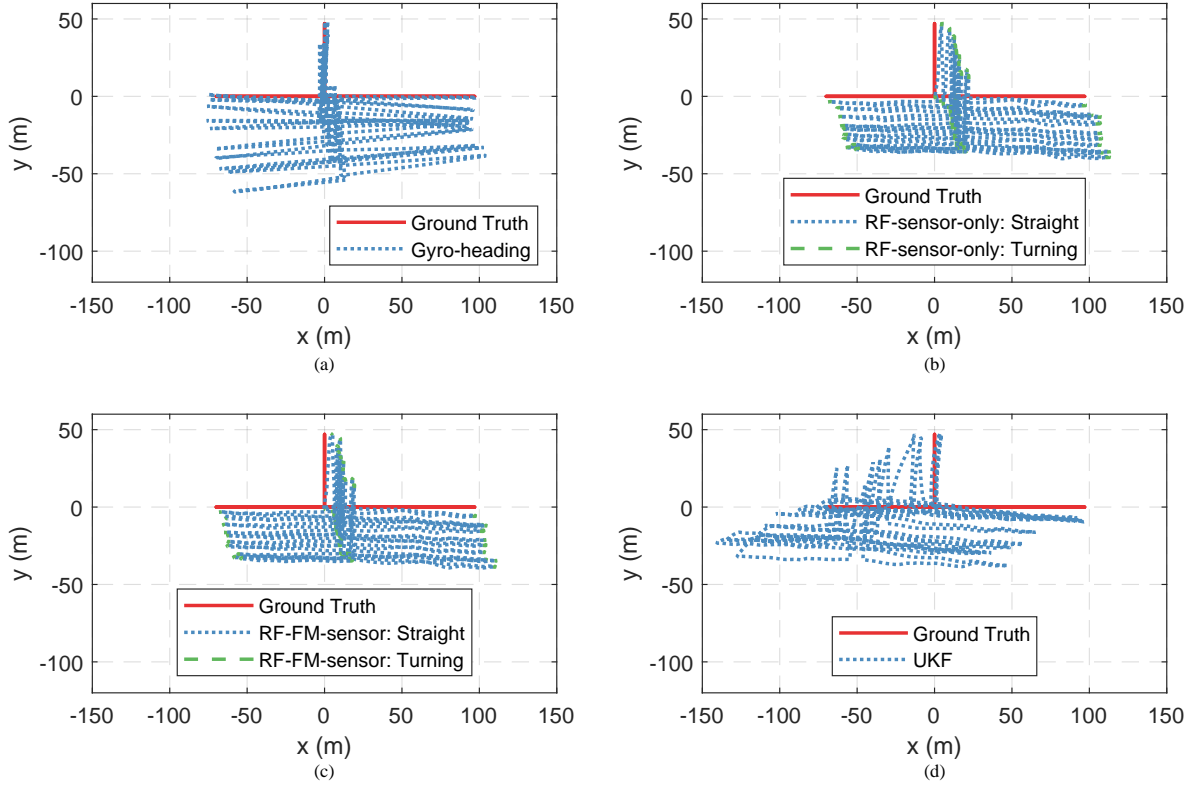[14] Z. Zhang, X. Meng, and J. Wu, "Quaternion-based kalman filter with

Fig. 18. Comparison of different trajectories at the third test site. (a) Trajectory by the gyro-heading method. (b) Trajectory by the RF-sensor-only method. (c) Trajectory by the RF-FM-sensor method. The blue dotted parts are detected straight-line segments and the green dash-dotted parts are detected turning segments.
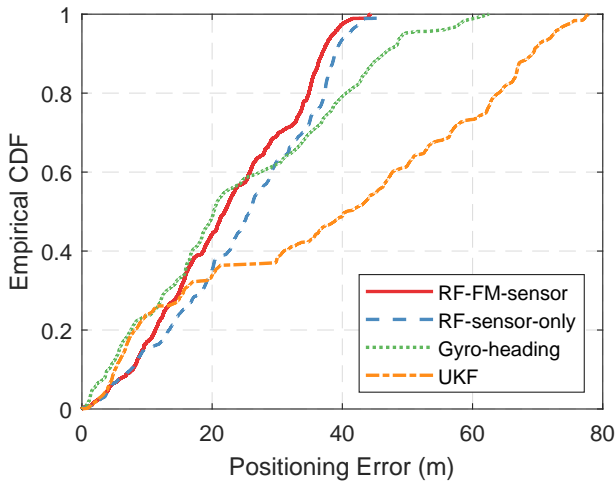

Fig. 19. Empirical error cumulative distribution functions of multiple trajectories at the third test site.

vector selection for accurate orientation tracking," *IEEE Transactions on Instrumentation and Measurement*, vol. 61, pp. 2817–2824, Oct. 2012.

[15] K. Abdulrahim, C. Hide, T. Moore, and C. Hill, "Using constraints for shoe mounted indoor pedestrian navigation," *Journal of Navigation*, vol. 65, no. 1, p. 1528, 2012.

[16] X. Yuan, S. Yu, S. Zhang, G. Wang, and S. Liu, "Quaternion-based unscented kalman filter for accurate indoor heading estimation using wearable multi-sensor system," *Sensors*, vol. 15, no. 5, pp. 10872–10890, 2015.

[17] Z. Zhang and X. Meng, "Use of an inertial/magnetic sensor module for pedestrian tracking during normal walking," *IEEE Transactions on Instrumentation and Measurement*, vol. 64, pp. 776–783, Mar. 2015.

[18] Y. Zhuang and N. El-Sheimy, "Tightly-coupled integration of WiFi and MEMS sensors on handheld devices for indoor pedestrian navigation," *IEEE Sensors Journal*, vol. 16, pp. 224–234, Jan. 2016.

[19] A. R. J. Ruiz, F. S. Granja, J. C. P. Honorato, and J. I. G. Rosas, "Accurate pedestrian indoor navigation by tightly coupling foot-mounted IMU and RFID measurements," *IEEE Transactions on Instrumentation and Measurement*, vol. 61, pp. 178–189, Jan. 2012.

[20] B. Krach and P. Roberston, "Cascaded estimation architecture for integration of foot-mounted inertial sensors," in *2008 IEEE/ION Position, Location and Navigation Symposium*, pp. 112–119, May 2008.

[21] N. Castaeda and S. Lamy-Perbal, "An improved shoe-mounted inertial navigation system," in *2010 International Conference on Indoor Positioning and Indoor Navigation*, pp. 1–6, Sept. 2010.

[22] A. Brajdic and R. Harle, "Walk detection and step counting on unconstrained smartphones," in *Proceedings of the 2013 ACM international joint conference on Pervasive and ubiquitous computing*, pp. 225–234, ACM, 2013.

[23] H. Weinberg, "Using the ADXL202 in pedometer and personal navigation applications," *Analog Devices AN-602 application note*, vol. 2, no. 2, pp. 1–6, 2002.

[24] A. R. Pratama, Widyawan, and R. Hidayat, "Smartphone-based pedestrian dead reckoning as an indoor positioning system," in *2012 International Conference on System Engineering and Technology (ICSET)*, pp. 1–6, Sept. 2012.

[25] J. W. Kim, H. J. Jang, D.-H. Hwang, and C. Park, "A step, stride and heading determination for the pedestrian navigation system," *Positioning*, vol. 1, no. 08, p. 0, 2004.

[26] H. Zhang, W. Yuan, Q. Shen, T. Li, and H. Chang, "A handheld inertial

pedestrian navigation system with accurate step modes and device poses recognition," *IEEE Sensors Journal*, vol. 15, pp. 1421–1429, Mar. 2015.

[27] J. Qian, L. Pei, J. Ma, R. Ying, and P. Liu, "Vector graph assisted pedestrian dead reckoning using an unconstrained smartphone," *Sensors*, vol. 15, no. 3, pp. 5032–5057, 2015.

[28] K. Abdulrahim, C. Hide, T. Moore, and C. Hill, "Aiding low cost inertial navigation with building heading for pedestrian navigation," *Journal of Navigation*, vol. 64, no. 2, p. 219233, 2011.

[29] K. Abdulrahim, C. Hide, T. Moore, and C. Hill, "Aiding MEMS IMU with building heading for indoor pedestrian navigation," in *2010 Ubiquitous Positioning Indoor Navigation and Location Based Service*, pp. 1–6, Oct 2010.

[30] J. Borenstein, L. Ojeda, and S. Kwanmuang, "Heuristic reduction of gyro drift for personnel tracking systems," *Journal of Navigation*, vol. 62, p. 4158, Jan. 2009.

[31] J. Borenstein and L. Ojeda, "Heuristic drift elimination for personnel tracking systems," *Journal of Navigation*, vol. 63, no. 4, p. 591606, 2010.

[32] P. Aggarwal, D. Thomas, L. Ojeda, and J. Borenstein, "Map matching and heuristic elimination of gyro drift for personal navigation systems in GPS-denied conditions," *Measurement Science and Technology*, vol. 22, no. 2, p. 025205, 2011.

[33] A. R. Jimnez, F. Seco, F. Zampella, J. C. Prieto, and J. Guevara, "Improved heuristic drift elimination (iHDE) for pedestrian navigation in complex buildings," in *2011 International Conference on Indoor Positioning and Indoor Navigation*, pp. 1–8, Sept 2011.

[34] A. Jiménez, F. Seco, F. Zampella, J. Prieto, and J. Guevara, "Improved heuristic drift elimination with magnetically-aided dominant directions (MiHDE) for pedestrian navigation in complex buildings," *Journal of Location Based Services*, vol. 6, pp. 186–210, Sept. 2012.

[35] L. E. Diez, A. Bahillo, S. Bataineh, A. D. Masegosa, and A. Perallos, "Enhancing improved heuristic drift elimination for wrist-worn PDR systems in buildings," in *2016 IEEE 84th Vehicular Technology Conference (VTC-Fall)*, pp. 1–5, Sept 2016.

[36] A. Popleteev, *Indoor positioning using FM radio signals*. PhD thesis, University of Trento, 2011.

[37] Y. Chen, D. Lymberopoulos, J. Liu, and B. Priyantha, "Fm-based indoor localization," in *Proceedings of the 10th international conference on Mobile systems, applications, and services*, pp. 169–182, ACM, 2012.

[38] V. Moghtadaiee, A. G. Dempster, and S. Lim, "Indoor localization using FM radio signals: A fingerprinting approach," in *2011 International Conference on Indoor Positioning and Indoor Navigation*, pp. 1–7, Sept. 2011.

[39] C. Huang, Z. Liao, and L. Zhao, "Synergism of INS and PDR in self-contained pedestrian tracking with a miniature sensor module," *IEEE Sensors Journal*, vol. 10, pp. 1349–1359, Aug. 2010.

[40] W. Kang and Y. Han, "Smartpdr: Smartphone-based pedestrian dead reckoning for indoor localization," *IEEE Sensors Journal*, vol. 15, pp. 2906–2916, May 2015.

[41] L. Breiman, "Random forests," *Machine Learning*, vol. 45, pp. 5–32, Oct 2001.

Li Cong received the M.S. degree from Harbin Engineering University in 2004, and the Ph.D. degree from Beihang University in 2008. She is currently an associate professor in the School of Electronic and Information Engineering, Beihang University. Her research interests include indoor positioning, integrated navigation and tactical navigation.

Honglei Qin received the B.S. degree in computer application from the Changchun Institute of Optical Precision Machinery, Changchun, China, in 1996, and the M.S. degree in electrical engineering from Harbin Institute of Technology, Harbin, China, in 1998, and the Ph.D. degree in navigation, guiding and control from Harbin Engineering University, Harbin, China, in 2001.

He is Leader of the CNT Laboratory of the Electronic Information and Engineering School at Beihang University, China. From July 2001 to May 2003, he worked in Beihang University as postdoctoral researcher. Now he is a full professor with School of Electronic and Information Engineering of Beihang University.

His main research interests comprise Global Navigation Satellite System (GNSS), Radio Navigation System, Integrated Navigation and Opportunity Signal Navigation.

Haidong Wang received the B.S. degree in electronic and information engineering from Beihang University, China, in 2016, where he is currently pursuing the M.S. degree with the School of Electronic and Information Engineering. His research interests include indoor positioning and sensor network.